

Transient Modeling of Thermal Degradation in Non-Charring Solids

YOUNGMIN SOHN^a, SEUNG WOOK BAEK^{a*} and
TAKASHI KASHIWAGI^b

^a*Korea Advanced Institute of Science and Technology, Aerospace Engineering Dept. 373-1 Kusung-dong, Yusung-ku, Taejon, South Korea* and ^b*National Institute of Standards and Technology, Fire Science Division, Gaithersburg, MD 20899*

(Received May 09, 1998; Revised January 26, 1999)

For a more extensive investigation of polymers, a better understanding of its gasification process is extremely essential. Especially compared with the extensive studies in the gas phase, the solid phase received rather little attention. Thus, the purpose of this paper is in its comparison of several modeling approaches for thermal degradation and systematic demonstration of the effects of basic assumptions on the model results, while taking account of in-depth radiation. For this object, this study has examined in more detail the degradation for a horizontally positioned polymer which is exposed to external radiation. After a preliminary study, three different solid degradation models were chosen from the literature, and their corresponding mass and energy conservation equations and boundary conditions were assembled. The in-depth non-gray as well as gray radiation was taken into account by solving relevant radiative transfer equation. In order to concentrate on the fundamental mechanisms of polymer degradation, gas phase reactions and subsequent heat feedback from the gas were neglected. This corresponds to a nitrogen environment. Various other parameters such as the polymer refractive index, polymer absorption coefficient, convective heat loss, solid fuel thickness and external radiative heat flux were changed to discuss their effects on the quantitative as well as qualitative change in the mass loss rate. While the effect of the solid fuel thickness on the mass loss rate was negligible for a thick sample, each parameter among the polymer refractive index, polymer absorption coefficient, convective heat loss, and external radiative heat flux incurred a non-negligible change in the results. Furthermore, the convection term in the energy equation, which is usually neglected in the in-depth pyrolysis by many other works, was shown to account for 29% decrease in the mass loss rate. Finally, depending on the solid degradation model used, the addition of gray radiation to the energy equation was shown to augment or diminish the mass loss rate. It was further enhanced by taking account of the non-gray radiation. This results from the fact that the inner solid is more quickly heated due to the far-reaching effects of radiation from the surface.

Keywords: condensed phase; polymer; degradation; in-depth radiation; mass loss rate; non-gray; PMMA

* Corresponding Author: E-Mail: swbaek@sorak.kaist.ac.kr

INTRODUCTION

The uses of polymers are so diverse that they are found in many applications in our living environment. Their production is expected to steadily increase in the future. Much attention is being paid to improve their fire safety. However, polymer combustion is such a complicated process that some physical phenomena still remain to be further investigated for a more detailed understanding. Compared with the efforts given to studies of the gas phase, the condensed phase is relatively less examined, as pointed out by Kashiwagi (1994) in a paper that reviews out current understanding of physical phenomena in polymer combustion.

For polymers, the pyrolysis rate is a primary component for characterizing flame spread and combustion. Various solid phase degradation models have been proposed so far and briefly summarized by Staggs (1997a). While the degradation of solid is assumed to occur infinitely rapidly at a critical temperature in some papers (Delichatsios and Chen (1993), Chen, et al. (1993) and Staggs (1997b)), there is also empirically based decomposition model (Parker (1985) as well as a solid-phase degradation model using the limited global in-depth reactions (Vovelle et al. (1987), Wichman and Atreya (1987) and Di Blasi and Wichman (1995)). Very recently, Staggs (1997a) extended previous works by developing a heat transfer model that incorporated a global single-step solid-phase reaction for the production of volatiles. A simple model for the mass transport inside solid is also included assuming that the polymer instantaneously fills the gaps left by in-depth volatilization.

A better understanding of physical processes that control the gasification of polymers is highly necessary for a study of combustion processes of polymers. But each pyrolysis rate model is limited to a specific case. Unlike previous studies, this current theoretical study examines the effects of various model assumptions on the degradation for a horizontally positioned polymer which is exposed to an external radiation directed normal to the polymer surface. Three different types of solid degradation model are considered. For each parameter, the quantitative and qualitative effects on retarding or enhancing the overall degradation are discussed to understand its fundamental role in the physical behavior. These parameters include the gray or non-gray in-depth radiation, polymer refractive index, polymer absorption coefficient, convective heat loss, solid fuel thickness and external radiative heat flux. In order to focus on the basic mechanism of polymers, the working environment is considered nitrogen so that a heat feedback from a gas phase reaction is neglected. These circumstances would eventually correspond to the Cone Calorimeter testing (Kashiwagi (1994)).

THEORETICAL MODEL

Governing Equations

As schematically shown in Fig. 1, the system is one-dimensional and unsteady. The PMMA fuel plate with 3 cm of thickness is horizontally positioned in the environment of inert nitrogen and one of solid surfaces is exposed to the external radiation source while the other surfaces are assumed to be adiabatic. In order to focus on the study of the condensed phase, the gas phase absorption by fuel vapors is neglected here, whereas the in-depth radiation but not scattering is taken into consideration in the solid phase. The radiative and convective heat losses to the surroundings are also included. Although the detailed transport mechanism of volatiles produced in the solid is not considered, the convective energy transport by volatiles is included.

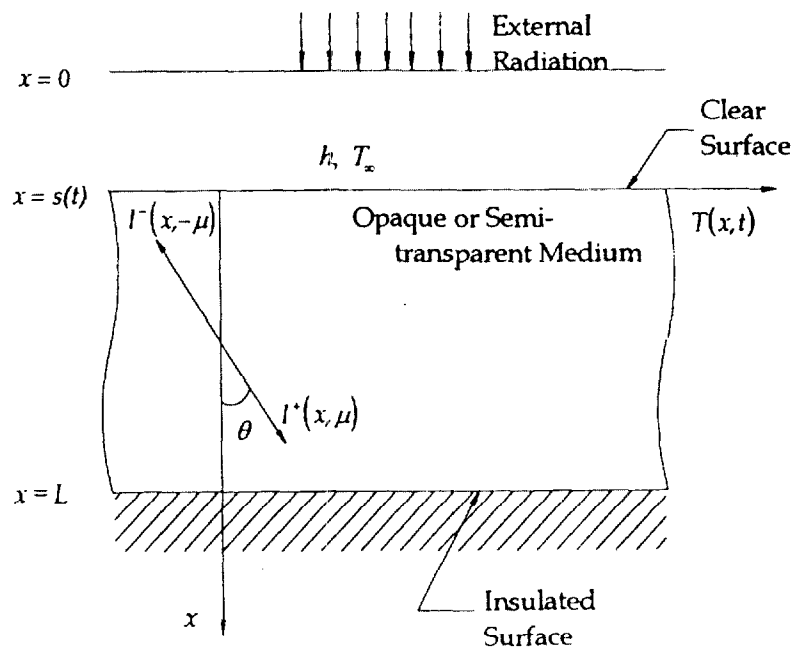


FIGURE 1 Schematic of the problem

First of all, based on the radiative characteristics of the PMMA, the model is referred to as either opaque or semi-transparent. Opaque PMMA will absorb and

partly reflect the external radiation on its surface only so that the radiation cannot penetrate into the solid. For semi-transparent PMMA, the external radiation can reach inside the solid. Furthermore, each opaque or semi-transparent model is again reorganized into three groups, A, B, or C according to the type of thermal degradation phenomenon

Model A assumes that the material is pyrolyzed only at the surface requiring a known pyrolysis temperature as well as heat of vaporization (Qian, et al. (1994)). For this case, it is impossible for the temperature anywhere in the solid to exceed T_p . Therefore, once the pyrolysis temperature is attained at the surface, the radiative heat supplied to the surface is then used for pyrolysis and heat redistribution inside the solid through conduction. For Model B, the thermal pyrolysis is also taking place only at the surface, but following one-step reaction approximated by the Arrhenius equation which depends on instantaneous surface temperature so that the fixed pyrolysis temperature is no longer employed (Baek and Kim (1997)). For Model C, the pyrolysis occurs not only at the surface of the solid, but also inside. In this case, a different Arrhenius form from that used in Model B is followed, since the pyrolysis term must be included in the energy equation (Vovelle et al. (1987)). Its local pyrolysis rate depends on the instantaneous local temperature.

In the following, the mass loss rate corresponding to each model above is represented for two types of radiative model, respectively.

For radiatively opaque solids ($\nabla \cdot q_r = 0$)

In this case, since the fuel surface is opaque to the external radiation, the divergence of radiative heat flux in the energy equation becomes zero, i.e., $\nabla \cdot q_r = 0$. Then, the mass loss rate becomes as follows:

For Model A:

$$\rho v = \frac{1}{H_p} \left[\varepsilon_w (q_e - \sigma T_w^4) + k_s \left. \frac{\partial T_s}{\partial x} \right|_w + h (T_\infty - T_w) \right] \quad (1)$$

For Model B:

$$\rho v = A_p \exp(-E_p/R_u T_w) \quad (2)$$

For Model C:

$$\rho v = \int_{s(t)}^L -\frac{d\rho_s}{dt} dx \quad (3)$$

where v is the regression rate of the surface and $s(t)$ is the surface location at time t . L is the location of the other adiabatic lower wall of the fuel plate. The first term on the right-hand side of the equation for Model A is the net radiative

heat flux to the fuel surface, the second term the conductive heat flux into the solid, the third one the convective heat loss.

For radiatively semi-transparent solids ($\nabla \cdot q_r \neq 0$)

In this case, since the fuel surface is semi-transparent to the external radiation, a non-zero divergence term of radiative heat flux is kept in the energy equation, i.e., $\nabla \cdot q_r \neq 0$ so that the mass loss rate becomes as follows:

For Model A:

$$\rho v = \frac{1}{H_p} \left[k_s \frac{\partial T_s}{\partial x} \Big|_w + h(T_\infty - T_w) \right] + \frac{1}{H_p} \int_{s(t)}^{x_m} \rho \frac{\partial H_s}{\partial t} dx \quad (4)$$

For Model B:

$$\rho v = A_p \exp(-E_p/R_u T_w) \quad (5)$$

For Model C:

$$\rho v = \int_{s(t)}^L -\frac{d\rho_s}{dt} dx \quad (6)$$

The second term on the right-hand side of Eq. (4) for Model A represents a mass loss rate due to the excessive sensible enthalpy over T_p in the mushy zone.

In the following the governing equations (Gandhi et al. (1986)) are cast only for radiatively semi-transparent solids with the thermal degradation Model C. Based on these, the other equations for the different models can be easily derived with proper modifications.

Continuity equation

$$\frac{\partial \rho_s}{\partial t} + \frac{\partial \dot{m}''}{\partial x} = 0 \quad (7)$$

Energy equation

$$\frac{\partial}{\partial t} (\rho_s C_s T_s) + \frac{\partial}{\partial x} (\dot{m}'' C_s T_s) = k_s \frac{\partial^2 T_s}{\partial x^2} + H_p \frac{d\rho_s}{dt} - \nabla \cdot q_r \quad (8)$$

Following Vovelle (1987), the thermal decomposition of the solid is governed by the following Arrhenius reaction rate kinetics

$$\frac{d\rho_s}{dt} = -\rho A_s \exp(-E_s/RT_s) \quad (9)$$

Note that the second term on the left-hand side and the second term on the right-hand side of equation (8) will be omitted when using thermal degradation Model A or B, since in these cases there is no in-depth thermal decomposition inside the solid.

Initial and Boundary Conditions

Initially the PMMA fuel plate is assumed to be held at room temperature. At time $t > 0$, the upper wall of the PMMA is exposed to the external radiation heat source. Then the initial and boundary conditions are as follows:

Initial condition:

$$\text{For Model A, B, and C: } T_s = T_i, 0 \leq x \leq L, t = 0$$

Boundary condition on the upper fuel surface, $x = s(t)$, $t > 0$

For radiatively opaque solids ($\nabla \cdot q_r = 0$)

For Model A: When $T_w < T_p$ ($= 630\text{K}$)

$$\varepsilon_w (q_e - \sigma T_w^4) + h(T_\infty - T_w) = -k_s \frac{\partial T_s}{\partial x} \quad (10)$$

When $T_w = T_p$

$$\varepsilon_w (q_e - \sigma T_w^4) - \rho v H_p + h(T_\infty - T_w) = -k_s \frac{\partial T_s}{\partial x} \quad (11)$$

For Model B:

$$\varepsilon_w (q_e - \sigma T_w^4) - \rho v H_p + h(T_\infty - T_w) = -k_s \frac{\partial T_s}{\partial x} \quad (12)$$

For Model C:

$$\varepsilon_w (q_e - \sigma T_w^4) + h(T_\infty - T_w) = -k_s \frac{\partial T_s}{\partial x} \quad (13)$$

For radiatively semi-transparent solids ($\nabla \cdot q_r \neq 0$)

For Model A: When $T_w < T_p$

$$h(T_\infty - T_w) = -k_s \frac{\partial T_s}{\partial x} \quad (14)$$

When $T_w = T_p$

$$-\rho v H_p + h(T_\infty - T_w) = -k_s \frac{\partial T_s}{\partial x} \quad (15)$$

For Model B:

$$-\rho v H_p + h(T_\infty - T_w) = -k_s \frac{\partial T_s}{\partial x} \quad (16)$$

For Model C:

$$h(T_\infty - T_w) = -k_s \frac{\partial T_s}{\partial x} \quad (17)$$

Boundary condition on the lower adiabatic wall, $x = L$, $t > 0$

For radiatively opaque solids ($\nabla \cdot q_r = 0$)

For Model A, B, and C:

$$\frac{\partial T_s}{\partial x} = 0 \quad (18)$$

For radiatively semi-transparent solids ($\nabla \cdot q_r \neq 0$)

For Model A, B, and C:

$$q_r - k_s \frac{\partial T_s}{\partial x} = 0 \quad (19)$$

The convective heat transfer coefficient h on the upper wall is estimated from an empirically correlated Nusselt number for a horizontal plate (McAdams (1954)).

Gray Radiation Model

The effect of radiative heat transfer in the semi-transparent model appears in the energy equation as the divergence of radiative heat flux $\nabla \cdot q_r$. In order to calculate it, the following radiative transfer equation for the two flux model needs to be solved. Scattering is neglected.

$$\mu \frac{\partial I^+}{\partial x} = aI_b - aI^+ \quad (0 \leq \theta \leq \pi/2) \quad (20)$$

$$-\mu \frac{\partial I^-}{\partial x} = aI_b - aI^- \quad (\pi/2 \leq \theta \leq \pi) \quad (21)$$

where I^+ and I^- are the forward and backward intensities, respectively and $\mu = \cos \theta$. Integrating the above equations over angle θ by introducing the Schuster-Schwarzschild approximation (Siegel & Howell (1992)) which assumes the isotropic intensity gives

$$\frac{1}{2} \frac{\partial I^+}{\partial x} = aI_b - aI^+ \quad (22)$$

$$-\frac{1}{2} \frac{\partial I^-}{\partial x} = aI_b - aI^- \quad (23)$$

The boundary conditions for the intensity are

$$I^+(s(t)) = \varepsilon_w q_c / \pi \quad \text{at the upper fuel surface} \quad (24)$$

$$I^-(L) = 0 \quad \text{at the lower adiabatic wall} \quad (25)$$

Using the boundary conditions above, the solutions to equation (22) and (23) can be obtained as follows

$$I^+(x) = I^+(s(t)) \exp(-2ax) + 2 \int_{s(t)}^x I_b(x^*) \exp[2a(x^* - x)] dx^* \quad (26)$$

$$I^-(x) = 2 \int_x^L I_b(x^*) \exp[2a(x - x^*)] dx^* \quad (27)$$

While the incident radiation G and radiative heat flux q_r can be expressed by

$$G = 2\pi \int_{-1}^1 I d\mu = 2\pi (I^+ + I^-) \quad (28)$$

$$q_r = 2\pi \int_{-1}^1 I \mu d\mu = \pi (I^+ - I^-) \quad (29)$$

the divergence of the radiative heat flux $\nabla \cdot q_r$ becomes

$$\nabla \cdot q_r = \frac{dq_r}{dx} = 4\pi a I_b - aG = 4\pi a I_b - 2\pi a (I^+ + I^-) \quad (30)$$

Physical and chemical properties used in this study are tabulated in Table I.

TABLE I Physical and chemical properties used. (Vovelle *et al.* (1987), Baek and Kim (1997) and Park and Tien (1990))

A_p [$kg\ m^{-2}s^{-1}$]	3.6×10^{12}
A_s [s^{-1}]	3.2×10^9
C_s [$J\ kg^{-1}\ K^{-1}$]	1.42×10^3
H_p [$J\ kg^{-1}$]	1.007×10^6
E_p [$J\ kg^{-1}\ mole^{-1}$]	1.8×10^8
E_s [$J\ mole^{-1}$]	1.42×10^5
k_s [$W\ m^{-1}\ K^{-1}$]	1.85×10^{-1}
ϵ_w	0.92
a [m^{-1}]	1.677×10^3

Non-Gray Radiation Model

In order to account for non-gray in-depth radiation absorption, Fourier transform infrared (FTIR) data for clear PMMA samples are used (Manohar (1995)). For soot-covered samples the transmittance was found to be negligible compared to that of the clear samples. The absorption coefficient data in the region 1800 to 6308 cm^{-1} are divided into 14 equal intervals. The absorption coefficient in each interval is assumed to be uniform. In the ranges below 1775 cm^{-1} and above

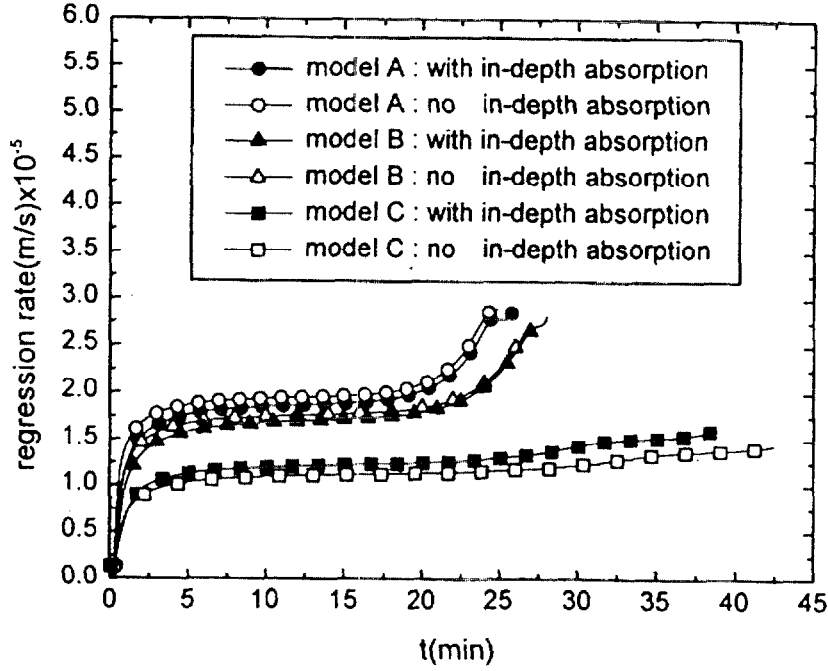


FIGURE 2 Comparison of regression rate with/without in-depth absorption

6250 cm^{-1} , the transmittance is considered negligible. For a non-gray calculation, the radiative transfer equation is solved for each band to obtain the spectral intensity and summed up for total intensity.

With the following spectral boundary conditions

$$I_v^+(s(t)) = \varepsilon_{w,v} q_{e,v} / \pi \quad \text{at the upper fuel surface} \quad (31)$$

$$I_v^-(L) = 0 \quad \text{at the lower adiabatic wall} \quad (32)$$

the forward and backward intensities are obtained by

$$I_v^+(x) = I_v^+(s(t)) \exp(-2a_v x) + 2 \int_{s(t)}^x I_{vb}(x^*) \exp[2a_v(x^* - x)] a_v dx^* \quad (33)$$

$$I_v^-(x) = 2 \int_x^L I_{vb}(x^*) \exp[2a_v(x - x^*)] a_v dx^* \quad (34)$$

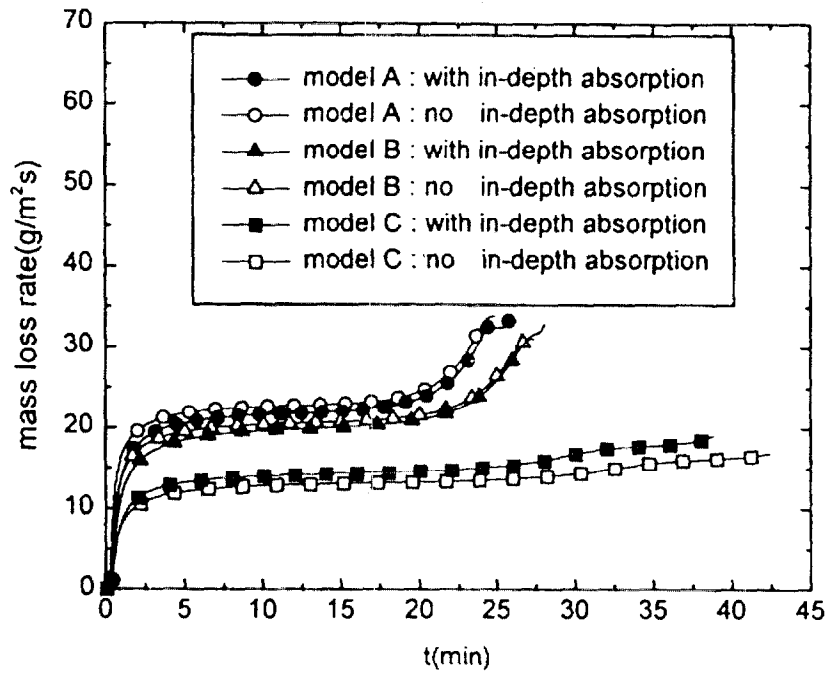


FIGURE 3 Comparison of mass loss rate with/without in-depth absorption

Since $\nabla \cdot q_{r,v} = \pi \left(\frac{\partial I_v^+}{\partial x} - \frac{\partial I_v^-}{\partial x} \right)$, total divergence of radiative heat flux becomes

$$\nabla \cdot q_r = \int_0^\infty \nabla \cdot q_{r,v} dv \quad (35)$$

Numerical Analysis

The unsteady governing equations are discretized by using implicit finite difference method. While the time derivative term is finitely differenced by forward differencing method, the upwind and central differencing methods are applied to the convective and diffusion terms, respectively. The fuel surface is determined using the simple interpolation when it is located within two grid points.

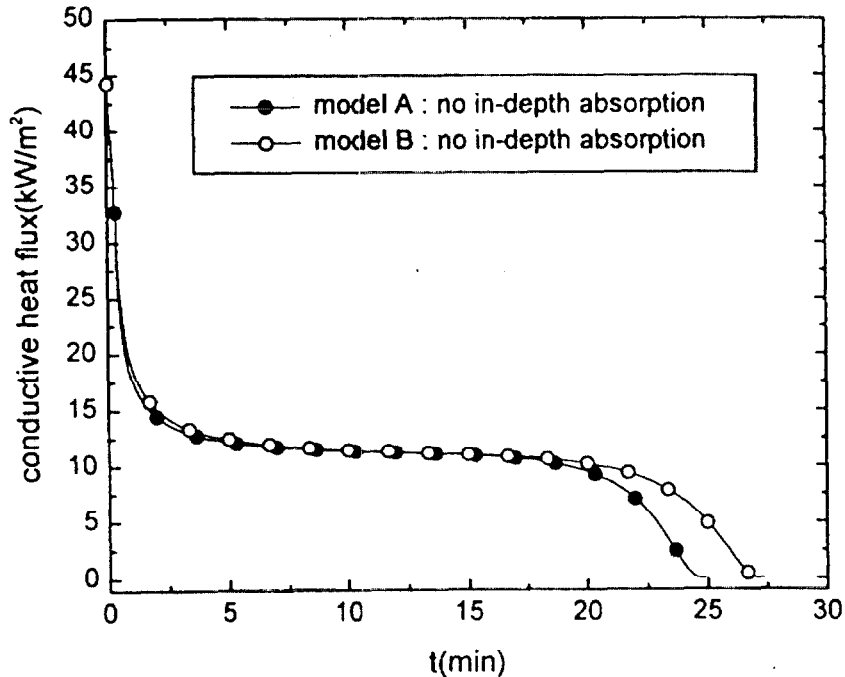


FIGURE 4 Comparison of conductive heat flux at PMMA surface

RESULTS AND DISCUSSION

The calculations for PMMA presented below are carried out until the ninety nine percent of solid thickness is pyrolyzed, considering the convective heat loss at the fuel surface. Unless specified otherwise, the thickness of fuel plate is 3 cm; the external radiative heat flux is 50 kW/m^2 ; the surface emissivity of PMMA is 0.92 for the opaque case.

Without in-depth radiation

First of all, as an elementary result for comparison with the other results, the solution without in-depth absorption is obtained. In Figs. 2 and 3, the surface regression rate and the mass loss rate are respectively plotted. It must be noted that these results may be dependent on the pre-exponential factor and activation energy used in each model. In this study, though, only the values as referenced in Table I are used. When the in-depth absorption is not included, the regression

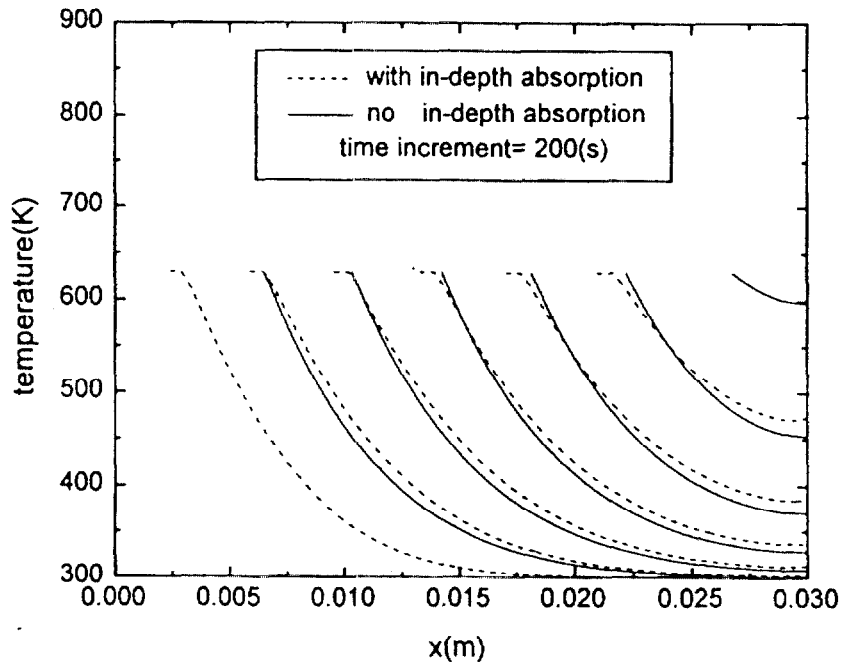


FIGURE 5 Temperature variation in PMMA for Model A with/without in-depth absorption

rate as well as the mass loss rate is the biggest for Model A and the smallest for Model C.

For the case of Model A, the incident external radiation on the PMMA surface increases the solid temperature. When the surface temperature reaches a pyrolysis temperature of 630 K in this study, this external radiative heat flux begins to pyrolyze the solid PMMA, still conducting the heat inward. This inward conductive heat flux decreases and then reaches a quasi-steady state as time goes on as shown in Fig. 4 in which the positive sign indicates the heat transfer from the fuel surface toward the inside. Simultaneously, both the mass loss rate and the surface regression rate increase and reach the quasi-steady state in which their increasing rate is very slow. Once the opposite surface of PMMA at $x=3\text{cm}$, held adiabatic, is affected by heat conduction from the surface, the temperature throughout the solid steadily increases as shown in Fig. 5. This again reduces the inward conductive heat flux at the fuel surface, thereby rapidly increasing again the surface regression rate and the mass loss rate. After the entire solid reaches the pyrolysis temperature, the inward conductive heat flux becomes zero as seen

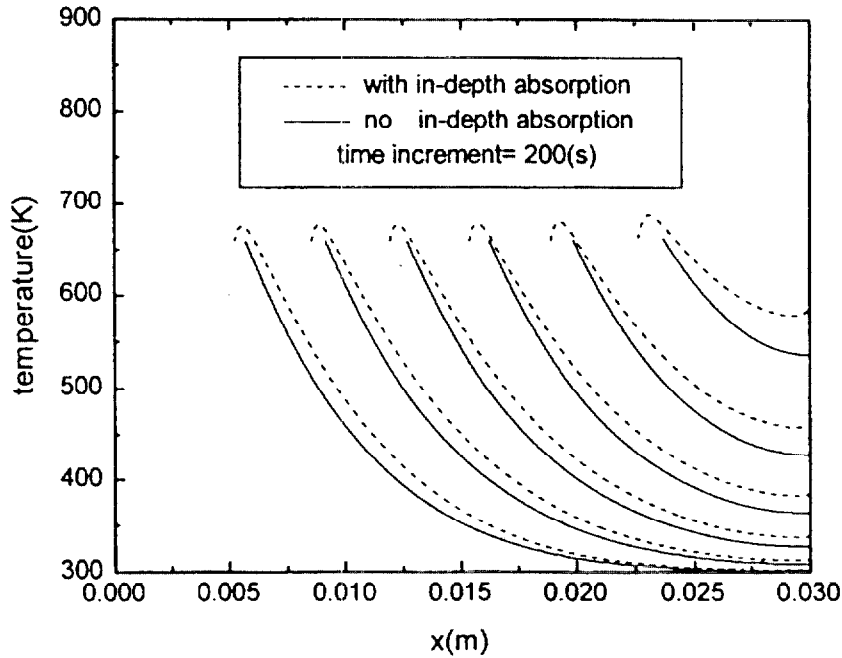


FIGURE 6 Temperature variation in PMMA for Model B with/without in-depth absorption

in Fig. 4 and the external radiative heat flux is only expended for the pyrolysis so that the mass loss rate finally would tend to reach another steady state value.

For the case of Model B, a similar behavior to that for Model A is observed in variations of the mass loss rate and the surface regression rate, except that they are smaller. The thermal pyrolysis in Model B occurs only at the surface, much like in Model A. Since the gas production rate is governed by the Arrhenius equation which depends on instantaneous surface temperature, the fixed pyrolysis temperature is no longer employed. However, as seen in Fig. 6, a quasi-steady temperature at 655 K still occurs. The case of Model C is unlike Model A and B in that the pyrolysis occurs throughout the solid according to the Arrhenius equation dependent on local temperature, so that the pyrolysis term as well as the convective term are included in the energy equation of the solid. In Figs. 2 and 3, the results for Model C are seen to be unlike those for Model A and B. The regression rate for Model C is the lowest of the three. Long after the quasi-steady state is reached, it very sluggishly rises again before arriving at another quasi-steady state and then rises once more, as the interior is heated up. However, as shown in

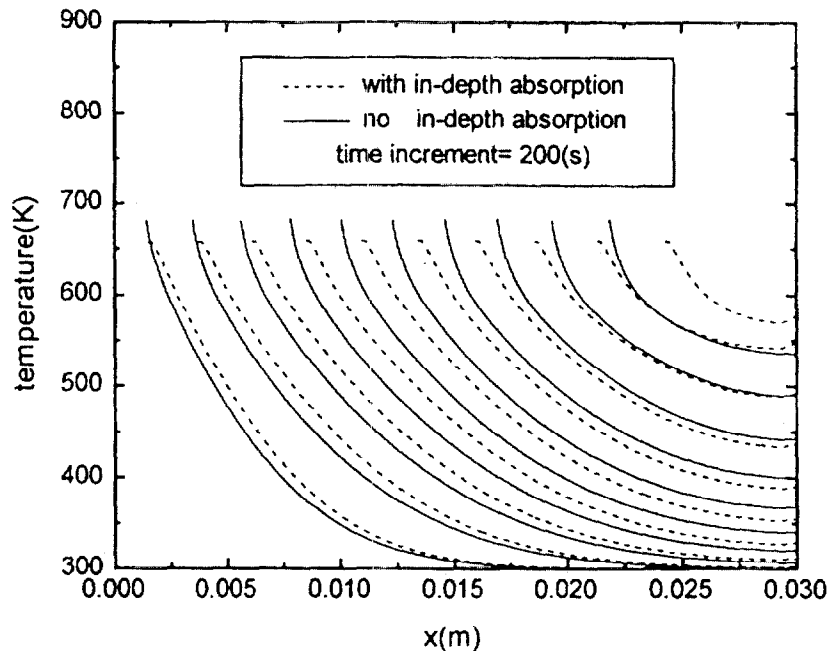


FIGURE 7 Temperature variation in PMMA for Model C with/without in-depth absorption

Fig. 7, the surface temperature does not steadily increase, even if it is free to rise in view of modeling. Instead, it is almost held at 680 K.

With gray in-depth radiation

The effects of gray in-depth absorption on the surface regression rate and the mass loss rate are represented and compared with other case in Figs. 2 and 3. The average absorption coefficient of 1677 m^{-1} obtained from FTIR data for clear PMMA samples (Manohar (1995)) has been used for calculation. For the thermal degradation Model A, the in-depth radiation is shown to reduce the mass loss rate for most of time, since more heat is transferred to inward so that the inner solid temperature increases faster than otherwise as seen in Fig. 5. Also for Model A, unlike the case without in-depth absorption, the second quasi-steady region distinctly appears in mass loss rate and regression rate as shown in Figs. 2 and 3. For Model B, the mass loss rate for the case with in-depth radiation is lower than that without in-depth radiation in the same way as for Model A. However, unlike Model A, the maximum temperature does not occur at the fuel sur-

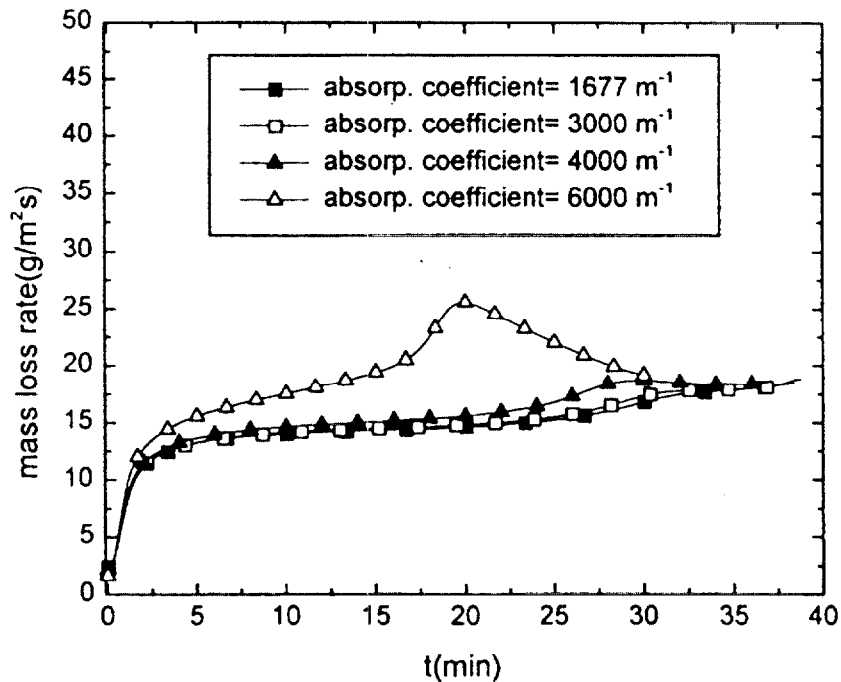


FIGURE 8 Effect of absorption coefficient on mass loss rate

face, but at the location beneath the surface, since due to the in-depth absorption, more heat is transferred to inward and absorbed therein as seen in Fig. 6. It was found for Model B that when all the inner solid is heated enough after a while, the in-depth radiation is shown to enhance the mass loss rate, exceeding the value for the case without in-depth radiation as shown in Figs. 2 and 3, since the total heat transfer from the surface towards inside is extensively reduced. For Model C, as the pyrolysis occurs throughout the solid depending on the local temperature, the higher temperature distribution along the solid with in-depth radiation results in a higher pyrolysis rate, even if the maximum temperature is lower than that without in-depth radiation as seen in Fig. 7.

It must be also noted that the adiabatic condition at the lower end wall does not necessarily mean zero temperature gradient at that location. Instead, an inverse temperature gradient is found. This results from the fact that a net summation of the radiative and conductive heat fluxes toward the wall must be zero to meet the adiabatic condition with in-depth radiation.

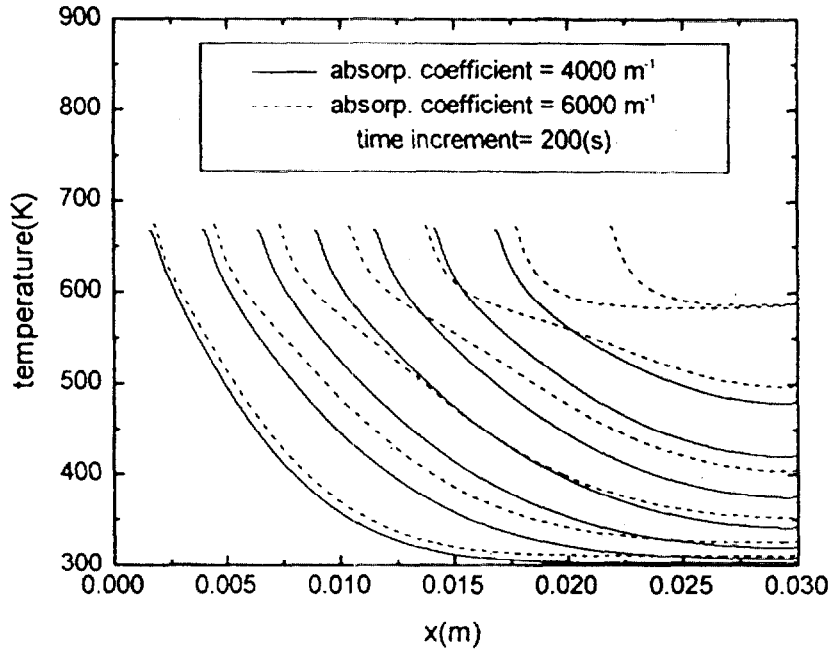


FIGURE 9 Effect of absorption coefficient on temperature variation

Effect of absorption coefficient

So far, the average of absorption coefficient of 1677 m^{-1} obtained from FTIR data has been used for calculation. In the following the absorption coefficient is arbitrarily changed to examine its effect while adopting the thermal degradation Model C. As shown in Fig. 8, the mass loss rate in general increases as the absorption coefficient increases. For the case for $a=6000 \text{ m}^{-1}$, it is observed that the mass loss rate increases and then decreases as time goes on. In order to find a specific reason, the temperature variations are plotted for $a=4000$ and 6000 m^{-1} in Fig. 9. It is seen that the inner solid for $a=6000 \text{ m}^{-1}$ is heated up much faster and the temperature distributions for times greater than 1200 s are similar. As previously mentioned, Model C assumes the pyrolysis takes place throughout the solid depending on the temperature. The decrease in the mass loss rate in Fig. 8 is therefore not due to the thermal behavior, but instead results from the reduction in the solid thickness during in-depth pyrolysis as time goes on. Consequently, there are two factors affecting the mass loss rate for Model C, namely, internal temperature and size. While the former is a controlling factor in the ini-

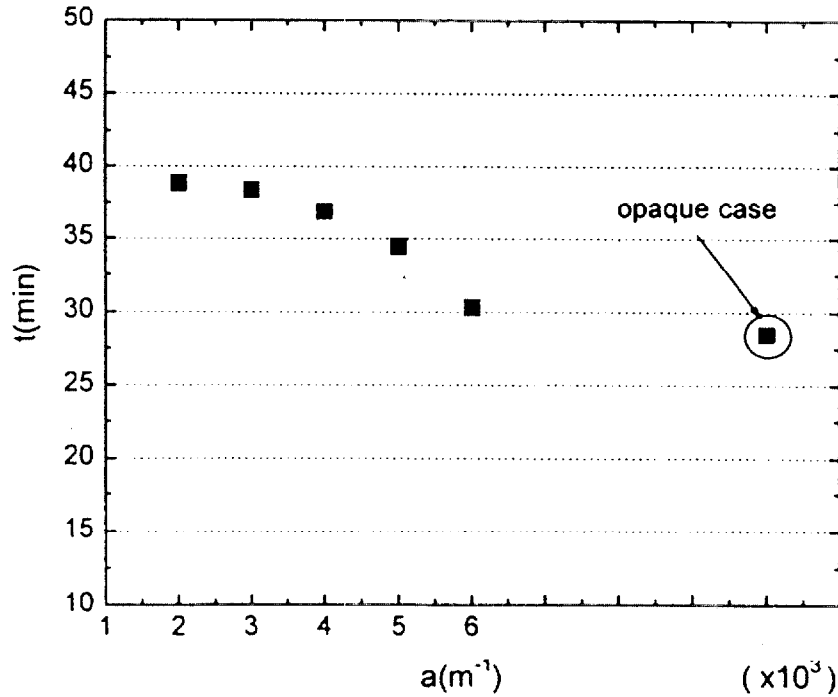


FIGURE 10 Effect of absorption coefficient on total pyrolysis time

tial stage, the latter dominates in the final stage. The larger the absorption coefficient, the more significant role does the size factor play in the final stage. The total pyrolysis time for a PMMA sample of 3 cm is represented in Fig. 10. It shows that the effect of the absorption coefficient plays a significant role in thermal degradation. The calculation with opaque surface is also included for comparison.

Effect of the convective heat loss on solid fuel surface

In previous results the solid fuel PMMA exposed to the external radiation was horizontally positioned, requiring the convective heat loss to be taken into consideration. The convective heat loss tends to lower the surface temperature. Now it is removed to inspect its effects. In Fig. 11 the results are compared for three different thermal degradation models. As expected, the mass loss rate increases when the convective heat loss on the fuel surface is not taken into account. The maximum increase is about 11%.

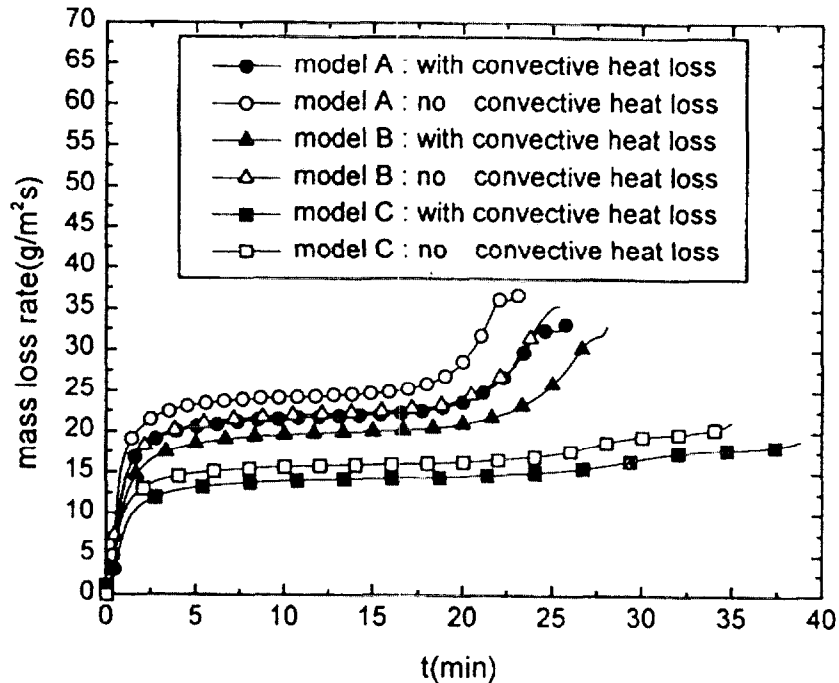


FIGURE 11 Effect of convective heat loss at solid surface on mass loss rate

Effect of the convective term in Model C

As noted earlier, Model C assumes that the pyrolysis occurs not only at the surface, but also inside the PMMA. The fuel vapor evolved inside migrates toward the surface, at which it is considered to be diffused out to the gas phase. The detailed mechanism for this is well beyond our current scope and is not elucidated here. Therefore, unlike Model A and B, this gaseous movement carries away heat so that the convective term is included in energy equation. In this section, the effect of this convective term on the mass loss rate is sought.

Figure 12 shows that the mass loss rate increases about 29 % when the convective term is omitted in the energy equation. This results from the fact that both the maximum temperature and the temperature gradient are higher without convection as shown in Fig. 13. The convection results in the supply of fuel vapor with a lower internal energy level to the higher internal energy zones, thereby dropping the temperature throughout the solid.

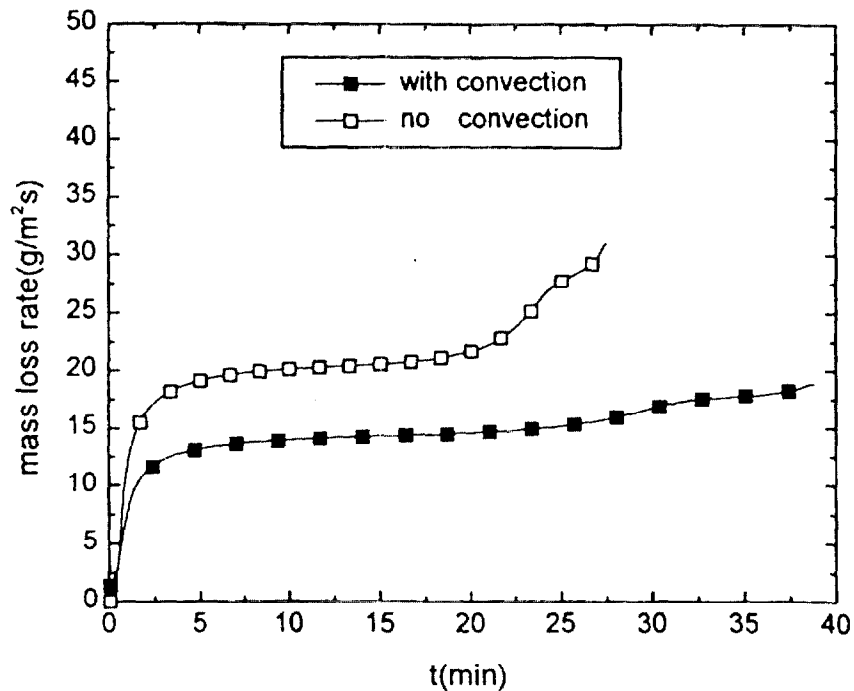


FIGURE 12 Effect of convective term in Model C on mass loss rate

Effect of refractive index of solid fuel

So far the refractive index of solid fuel was set to 1.0. The effect of different values of refractive index is illustrated using Model C in Fig. 14. As the refractive index increases to 1.2 and 1.5, the mass loss rate decreases by 11 % and 30% respectively. This is due to reductions in both the maximum temperature at the fuel surface and the temperature gradient inside the solid as the refractive index increases. In Fig.15, the temperature variation owing to the change of refractive index is plotted.

Effect of solid fuel thickness

The effect of PMMA thickness on the mass loss rate is plotted with Model C in Fig. 16 while the external radiative heat flux is set to 50 kW/m^2 . The time required for the mass loss rate to move from the first quasi-steady state to the second state increases as the thickness increases, whereas the mass loss rate for

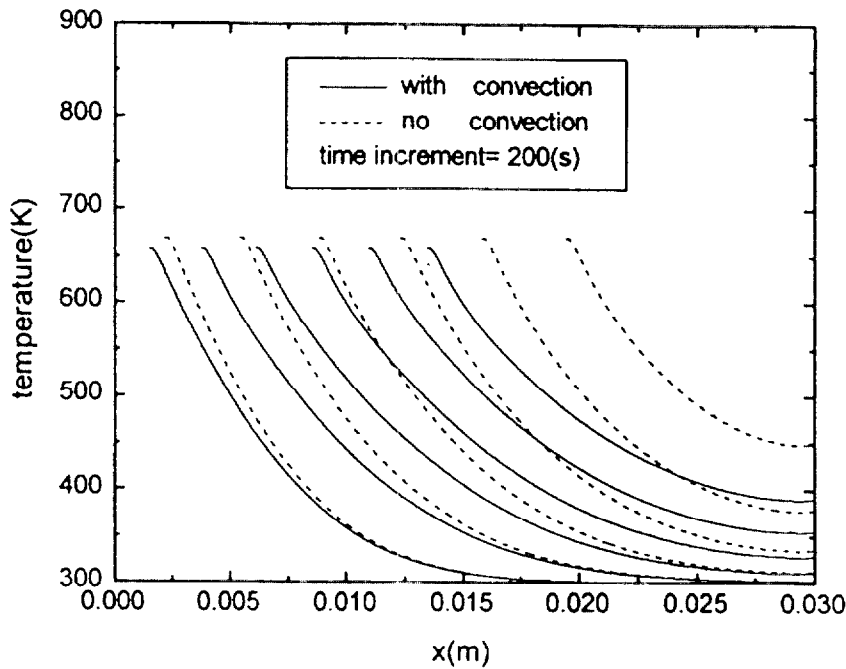


FIGURE 13 Effect of convective term in Model C on temperature variation

the first and second quasi-steady state seems not to be affected by the change of fuel thickness.

Effect of external radiative heat flux

While the PMMA thickness is set to 3 cm, the external radiative heat flux is varied from 30 up to 100 kW/m² using Model C in Fig. 17. The mass loss rate for the first and second quasi-steady state is observed to strongly depend on the external radiative heat flux. The mass loss rate for the first quasi-steady state increases as the external radiative heat flux increases. While the second quasi-steady state is distinctively recognized for 50 kW/m², it is almost uncertain for 100 kW/m² and it does not exist for 30 kW/m².

Effect of non-gray radiation

Finally, using Model C, the non-gray effect is taken into consideration and compared with gray cases for three absorption coefficients of 1677, 4000 and

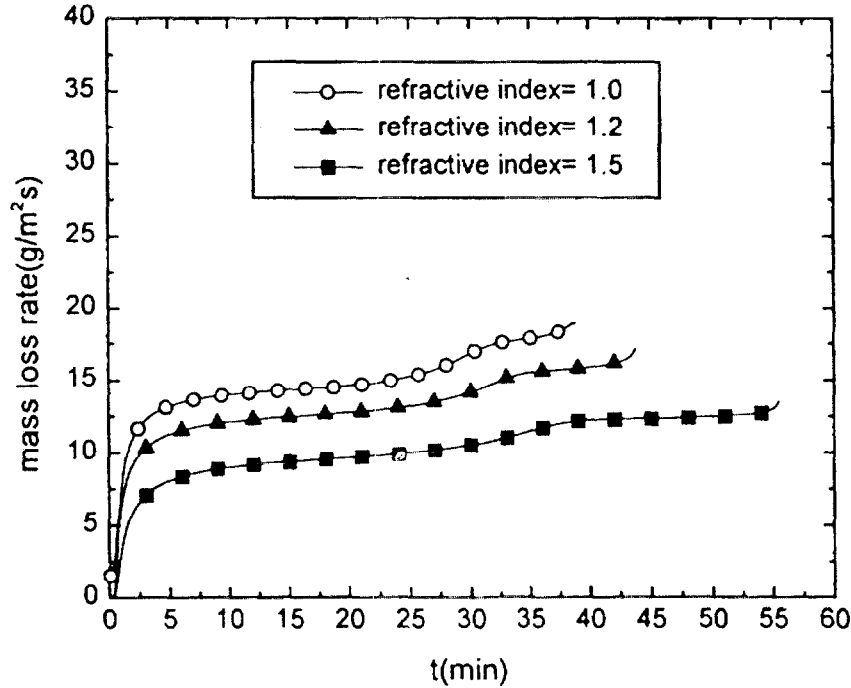


FIGURE 14 Effect of refractive index on mass loss rate

5000 m^{-1} . For non-gray absorption coefficients, the FTIR data for clear PMMA samples by Manohar (1995) are adopted. As shown in Fig. 18, the increasing rate of mass loss rate for the non-gray case is so high that the first and second quasi-steady states do not clearly occur and then the mass loss rate drops fast, since its thickness shrinks quickly. This is because the inner solid is heated up fast due to the non-gray radiation effects as seen in Fig. 19.

CONCLUSIONS

In this paper, the degradation of a horizontally positioned polymer exposed to an external radiation was investigated in the absence or presence of in-depth radiative absorption using three solid degradation models proposed in the literature. Inclusion of in-depth radiation is a genuine feature in this work. The effects of various model parameters on the degradation were also discussed.

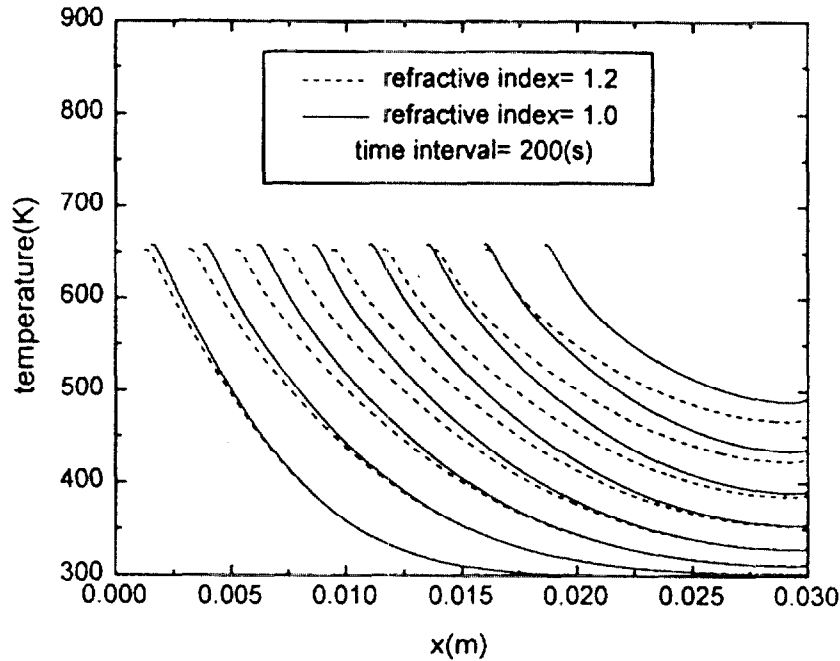


FIGURE 15 Effect of refractive index in Model C on temperature variation

Depending on the solid degradation model, the behavior of mass loss rate with time was found to vary moderately. Likewise, the inclusion of gray radiation enhanced the mass loss rate for Model C, while it is reduced for Model A and B. Addition of the non-gray radiation to Model C further intensified the mass loss rate, since the inner solid temperature increases more rapidly due to the far-reaching effects of radiation.

When the polymer refractive index, polymer absorption coefficient, convective heat loss, and external radiative heat flux were varied individually, non-negligible changes were observed in the mass loss rate. The solid fuel thickness did not affect the quasi-steady-state values of the mass loss rate, only the timing.

The convection term in the energy equation, which is often neglected in modeling, was found to account for a 29% decrease in the mass loss rate. This term should therefore not be neglected in further work.

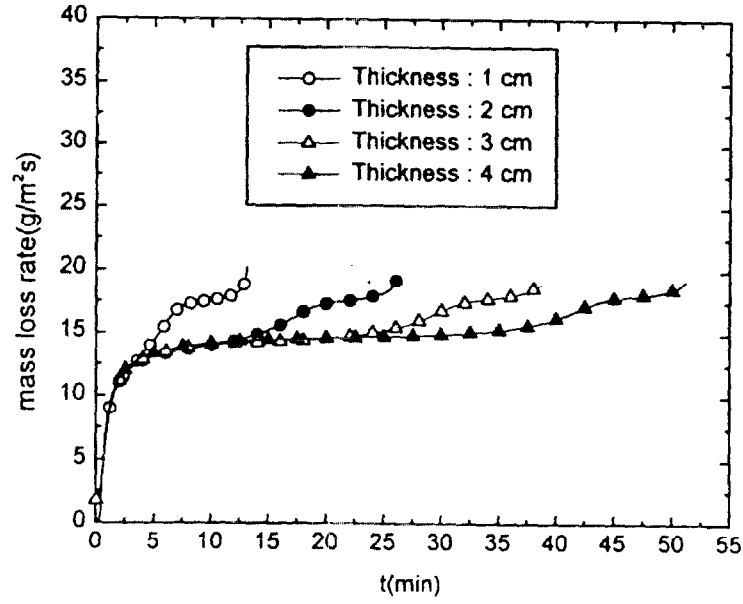


FIGURE 16 Effect of solid thickness on mass loss rate

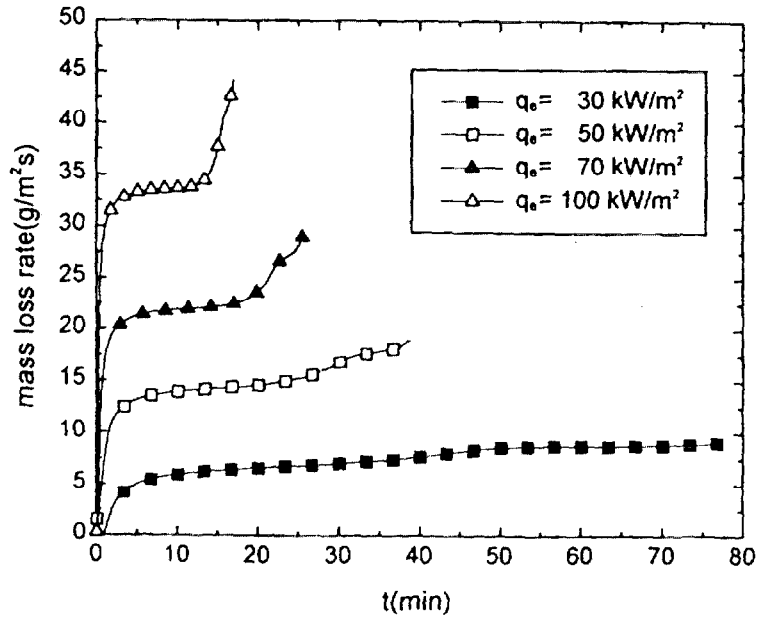


FIGURE 17 Effect of external radiative heat flux on mass loss rate

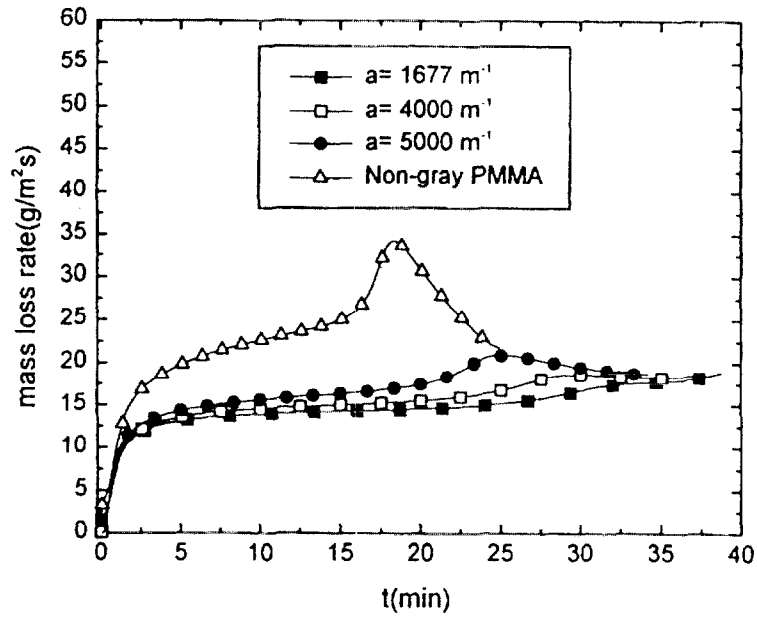


FIGURE 18 Comparison of mass loss rate for gray and non-gray PMMA

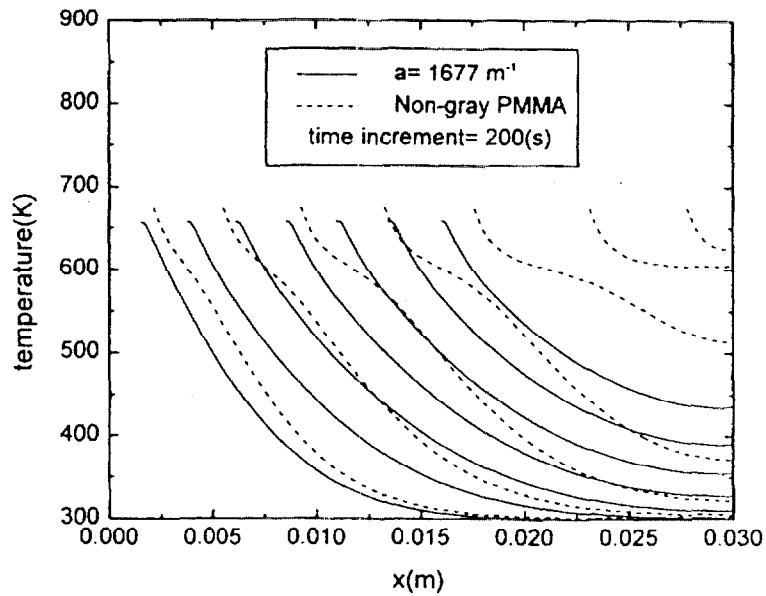


FIGURE 19 Comparison of temperature variation for gray and non-gray PMMA

NOMENCLATURE

a	absorption coefficient of solid, [m^{-1}]
A_p	pre-exponential factor for Model B, [$kg\ m^{-2}s^{-1}$]
A_s	pre-exponential factor for Model C, [s^{-1}]
C_s	specific heat of solid, [$J\ kg^{-1}\ K^{-1}$]
E_p	activation energy for Model B, [$J\ kg^{-1}\ mole^{-1}$]
E_s	activation energy for Model C, [$J\ mole^{-1}$]
ϵ_w	emissivity of PMMA surface
G	incident radiation, [$W\ m^{-2}$]
h	heat transfer coefficient, [$W\ m^{-2}K^{-1}$]
H_s	sensible enthalpy in mushy zone, [$J\ kg^{-1}$]
H_p	enthalpy of pyrolysis, [$J\ kg^{-1}$]
I	radiation intensity, [$W\ sr^{-1}\ m^{-2}$]
k_s	thermal conductivity of solid, [$W\ m^{-1}\ K^{-1}$]
L	thickness of PMMA, [m]
\dot{m}''	pyrolyzates mass flux for Model C, [$kg\ m^{-2}s^{-1}$]
q	radiative heat flux, [$W\ m^{-2}$]
R	specific gas constant, [$J\ K^{-1}mole^{-1}$]
R_u	universal gas constant, [$J\ kg^{-1}\ K^{-1}\ mole^{-1}$]
$s(t)$	position of PMMA surface, [m]
T_s	temperature of solid, [K]
T_p	pyrolysis temperature for Model A, [K]
t	time, [s]
v	regression rate, [$m\ s^{-1}$]
x	distance, [m]
x_m	distance from surface to the end of Mushy zone, [m]
θ	angle of directional radiation
ν	wave number, [m^{-1}]; also, spectral when subscripted
ρ	original density of solid, [$kg\ m^{-3}$]
ρ_s	in-depth density of solid, [$kg\ m^{-3}$]
σ	stefan-Boltzmann constant, [$Wm^{-2}K^{-4}$]

Subscripts

b	blackbody
e	external
i	initial
r	radiative

∞ ambient

w surface

Superscripts

+ forward

- backward

References

- Baek, S.W. and Kim, T.Y. (1997). Ignition phenomenon of solid fuel in a confined rectangular enclosure. *Int. J. Heat Mass Transfer*, **40**, p. 89.
- Delichatsios, M.A. and Chen, Y. (1993). Asymptotic, approximate and numerical solutions for the heatup and pyrolysis of materials including reradiation losses. *Comb. and Flame*, **92**, p. 292.
- Chen, Y., Delichatsios, M.A., and Motevalli, V. (1993). Material pyrolysis properties, part I: An integral model for one-dimensional transient pyrolysis of charring and non-charring materials. *Combust. Sci. and Tech.*, **88**, p. 309.
- Di Blasi, C. and Wichman, I.S. (1995). Effects of solid-phase properties on flames spreading over composite materials. *Comb. and Flame*, **102**, p. 229.
- Gandhi, P. D. and Kanury, A. M. (1986) Criterion for spontaneous ignition of radiantly heated organic solids. *Combust. Sci. and Tech.*, **50**, p. 233.
- Kashiwagi, T. (1994). Polymer combustion and flammability-role of the condensed phase. *25th Symp.(Int.) on Combustion*, The Combustion Institute, p. 1423.
- Parker, W.J. (1985). NBSIR 85-3163.
- Manohar, S.S., Kulkarni, A. K. and Thynell, S. T. (1995). In-depth absorption of externally incident radiation in nongray media". *ASME Journal of Heat Transfer*, **117**, p. 146.
- McAdams, W. H. (1954). *Heat Transmission*, 3rd ed., Chapter 7, McGraw-Hill, New York.
- Park, S. H. and Tien, C. L. (1990). Radiation induced ignition of solid fuels. *Int. J. Heat Mass Transfer*, **33**, p. 1511.
- Qian, C., Ishida, H. and Saito, K. (1994). Upward flame spread along PMMA vertical corner walls. *Comb. and Flame*, **99**, p. 331.
- Siegel, R. and Howell, J. R. (1992) *Thermal Radiation Heat Transfer*. Hemisphere Publishing Corporation, 3rd ed.
- Staggs, J.E.J. (1997a). A theoretical investigation into modelling thermal degradation of solids incorporating finite rate kinetics. *Combust. Sci. and Tech.*, **123**, p. 261.
- Staggs, J.E.J. (1997b). A discussion of modelling idealized ablative materials with particular reference to fire testing. *Fire Safety J.*, **28**, p. 47.
- Vovelle, C., Delfau, J. Reuillon, M., Bransier, J. and Laraqui, N. (1987). Experimental and numerical study of thermal degradation of PMMA. *Combust. Sci. and Tech.*, **53**, p. 187.
- Wichman, I.S. and Atreya, A. (1987). A simplified model for the pyrolysis of charring materials. *Comb. and Flame*, **68**, p. 231.